

Experimental Realization of Room Temperature Topological Hall Effect in Kagome Antiferromagnet

Achintya Low, Susanta Ghosh, Sayan Routh, and S. Thirupathaiah*

Department of Condensed Matter and Materials Physics,

S . N. Bose National Centre for Basic Sciences, JD Block, Sector 3, Salt Lake, Kolkata-700106

Magnetic topological semimetals are the manifestations of interplay between electronic and magnetic phases of the matter, leading to peculiar characteristics such as the anomalous Hall effect (AHE) and topological Hall effect (THE). Mn_3Sn is a time-reversal symmetry broken (TRS) magnetic Weyl semimetal showing topological characteristics within the Kagome lattice network. In this study, for the first time, we uncover large and pure topological Hall effect in Mn_3Sn at the room temperature, which is gradually suppressed by Fe doping at the Mn site of $\text{Mn}_{3-x}\text{Fe}_x\text{Sn}$. We further identify that the topological properties of these systems are highly anisotropic. These findings promise the realization of potential topotronic applications at room temperature.

Hall effect is one of the pioneering discoveries in condensed matter physics [1], gained a lot of attentiveness both from the fundamental and technological applications [2, 3]. Specifically, in the fundamental science, the Hall effect branched into various exotic phenomena such as the spin Hall effect (SHE) [4], the quantum Hall effect (QHE) [5–7], the anomalous Hall effect (AHE) [8], and the recently emerging topological Hall effect in helimagnets. Particularly, the topological Hall effect is a direct manifestation of real-space Berry phase acquired by the conduction electrons moving around the topologically stable knots, also called the skyrmions, in chiral spin structures [9–11]. Topological spin structures in helimagnets are driven by the geometrical frustration in triangular lattice or Dzyaloshinskii-Moriya interaction (DMI) in the absence of centrosymmetry of the crystal [12–17]. There exists several geometrically frustrated Kagome systems such as $\text{Co}_3\text{Sn}_2\text{S}_2$ [18, 19], Fe_3Sn_2 [20], EuCd_2As_2 [21] and non-centrosymmetric crystals such as the cubic B20 chiral magnets MnSi [22], FeGe [23], MnGe [24], Cu_2OSeO_3 [25], and Mn_2RhSn [26] showing topological Hall effect. Importantly, most of these magnetic topological systems show THE besides the magnetization driven anomalous Hall effect hindering the potential applications of THE in the topological electronics [27–29]. Thus, finding materials merely with topological Hall effect is desirable for the technological applications.

In this letter, we report on the topological Hall effect of $\text{Mn}_{3-x}\text{Fe}_x\text{Sn}$ ($x=0, 0.2, 0.25$, and 0.35) single crystals. Our studies show a large and pure room-temperature topological Hall effect with topological Hall resistivity $\rho_{xy}^T \approx 2 \mu\Omega\text{-cm}$ in Mn_3Sn at a low critical field of 0.3 T . To our knowledge, no other system shows such a pure and large THE signal at room temperature in its bulk form except Gd_2PdSi_3 which shows THE, with negligible AHE signal, but only at very low temperatures ($< 25\text{K}$) [30]. The value of ρ_{xy}^T increases further to $2.3 \mu\Omega\text{-cm}$ with decreasing temperature down to 260 K , but abruptly disappears below 260 K due to magnetic reorientation from

coplanar AFM to spin-spiral structure [31, 32]. We uncover highly anisotropic topological properties of these systems at room temperature. That means, anomalous Hall effect (AHE) has been noticed in the zx -plane, while the topological Hall effect has been noticed in xy -plane. Moreover, the room-temperature THE decreases with increasing Fe doping and it is almost suppressed by the Fe doping of $x=0.35$. Additionally, low temperature topological properties emerge by Fe doping. In the below, we explore in detail our experimental findings.

Single crystals of $\text{Mn}_{3-x}\text{Fe}_x\text{Sn}$ were prepared by the self-flux method as reported in [31, 33]. See supplementary information for additional details on the experimental procedure and sample characterization. Electrical resistivity measured along the a -axis (ρ_{xx}) plotted as a function of temperature in Fig. 1(c) for both Mn_3Sn and $\text{Mn}_{2.8}\text{Fe}_{0.2}\text{Sn}$. From Fig. 1(c) we can observe that the ρ_{xx} resistivity of the parent compound shows a metallic nature, and interestingly for the first time, we find a hump-like structure at around 260 K [shown in the inset of Fig. 1 (c)], whereas, in the case of Fe doped $\text{Mn}_{2.8}\text{Fe}_{0.2}\text{Sn}$, the resistivity decreases with increasing temperature which is a kind of bad-metallic behaviour [34]. Similarly, electrical resistivity measured along the c -axis (ρ_{zz}) plotted as a function of temperature in Fig. 1(d) for both Mn_3Sn and $\text{Mn}_{2.8}\text{Fe}_{0.2}\text{Sn}$. As can be seen from the ρ_{zz} resistivity data, both parent and Fe doped systems show metallic behavior at low temperatures except for a significant increase in the impurity resistivity from $0.3 \text{ m}\Omega\text{-cm}$ to $0.63 \text{ m}\Omega\text{-cm}$ with Fe doping. Further, we observe a *kink* at around 260 K in Mn_3Sn which has been ascribed earlier to the spin structure reorientation of Mn atoms from a high-temperature noncollinear inverse triangular structure to a low-temperature noncoplanar spiral structure [31, 32]. But with Fe doping, we find that the spin reorientation transition temperature decreased to 125 K at which the *kink* has been observed from the ρ_{zz} resistivity of $\text{Mn}_{2.8}\text{Fe}_{0.2}\text{Sn}$ as shown in Fig. 1 (d). Inset in Fig. 1 (d) shows thermal hysteresis in the ρ_{zz} resistivity of Mn_3Sn

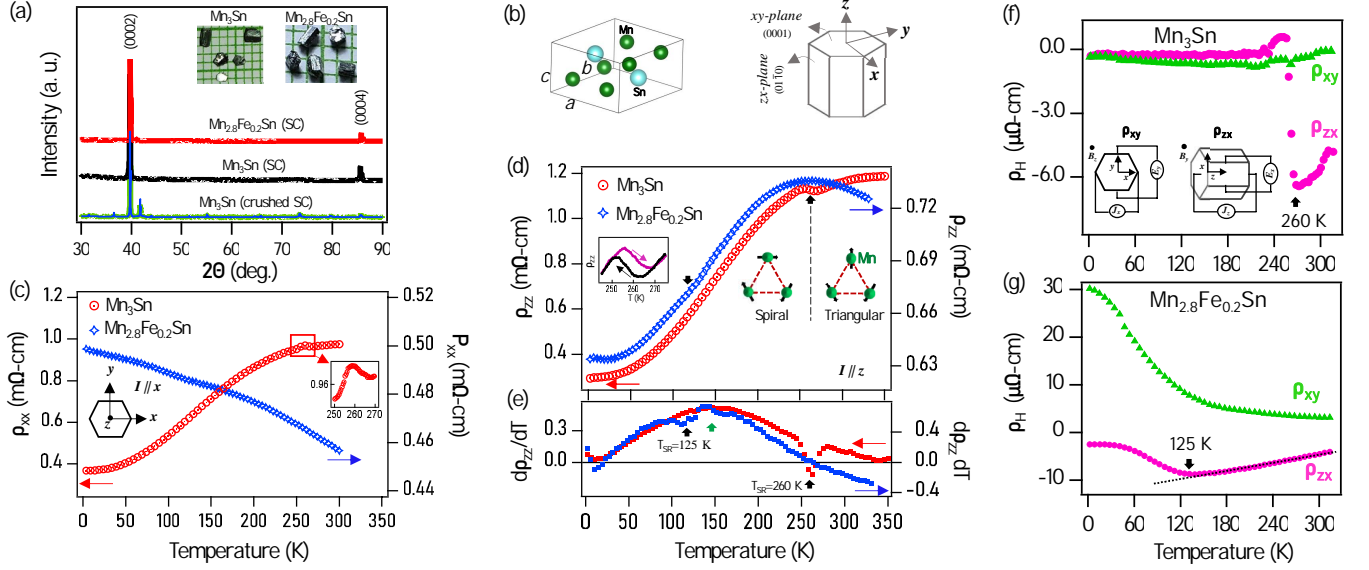


Figure 1. (a) Powder XRD data from crushed single crystals of Mn_3Sn , single crystal of Mn_3Sn , and $\text{Mn}_{2.8}\text{Fe}_{0.2}\text{Sn}$. Inset in (a) shows photographic image of Mn_3Sn and $\text{Mn}_{2.8}\text{Fe}_{0.2}\text{Sn}$ single crystals. Left-panel in (b) shows primitive unit cell of the hexagonal crystal structure of Mn_3Sn and the right-panel in (b) defines the crystal planes, zx -plane (0110) and xy -plane (0001) on the hexagonal unit cell. (c) Resistivity measured along the a -axis, ρ_{xx} , as a function of temperature is plotted for both Mn_3Sn and $\text{Mn}_{2.8}\text{Fe}_{0.2}\text{Sn}$. (d) Resistivity measured along the c -axis, ρ_{zz} , as a function of temperature is plotted for both Mn_3Sn and $\text{Mn}_{2.8}\text{Fe}_{0.2}\text{Sn}$. Right-side inset in (d) shows schematic representation of the spin-reorientation above and below the transition temperature of 260 K for Mn_3Sn and 125 K for $\text{Mn}_{2.8}\text{Fe}_{0.2}\text{Sn}$. Left-side inset in (d) shows thermal hysteresis of the resistivity, ρ_{zz} (T), between heating and cooling cycles of data collection on Mn_3Sn . (e) First derivative of ρ_{zz} with respect to the temperature. (f) xy -plane (ρ_{xy}) and zx -plane (ρ_{zx}) Hall resistivity measured as a function of temperature from Mn_3Sn with a magnetic field of 1 T applied parallel and perpendicular to the c -axis. Schematics in (f) show the measuring geometries used for recording the data of ρ_{xy} and ρ_{zx} . (g) Similar data of (f) but measured from $\text{Mn}_{2.8}\text{Fe}_{0.2}\text{Sn}$.

taken around 260 K between heating and cooling cycles. Thermal hysteresis in the ρ_{zz} resistivity is consistent with the previous report on Mn_3Sn except that it was found at 270 K [32] and 275 K [31]. Such a thermal hysteresis is attributed to the first-order type magnetic transition from triangular to spiral structure in this system [31]. On the other hand, we do not observe such a thermal hysteresis in the ρ_{zz} resistivity of $\text{Mn}_{2.8}\text{Fe}_{0.2}\text{Sn}$ despite having the magnetic transition at around 125 K.

To pinpoint the spin-reorientation transition temperature (T_{SR}), we plotted $d\rho_{zz}/dT$ as a function of temperature as shown in Fig. 1 (e). From the first derivative, we can reaffirm $T_{SR}=260$ K for Mn_3Sn and 125 K for $\text{Mn}_{2.8}\text{Fe}_{0.2}\text{Sn}$. In addition, we also observe a decrease in $d\rho_{zz}/dT$ with increasing T for both systems below 10 K possibly due to weak local potentials at low temperatures [35] and above 143 K due to an electronic phase transition. Eventually, $d\rho_{zz}/dT$ becomes zero at 265 K and beyond this temperature, it is negative for $\text{Mn}_{2.8}\text{Fe}_{0.2}\text{Sn}$. That means, $\text{Mn}_{2.8}\text{Fe}_{0.2}\text{Sn}$ shows a metal-insulator (MI) transition at around 265 K. On the other hand, in Mn_3Sn , the MI transition seems to be happening at much-elevated temperatures as $d\rho_{zz}/dT$ approaches zero at around 345 K [36]. To emphasize here, Mn_3Sn shows nearly isotropic resistivity between a and c axes,

while $\text{Mn}_{2.8}\text{Fe}_{0.2}\text{Sn}$ shows a large resistivity anisotropy.

Fig. 1(f) depicts Hall resistivity in the xy -plane (ρ_{xy}) and in the zx -plane (ρ_{zx}) plotted as a function of temperature from Mn_3Sn measured with a magnetic field of 1 T applied parallel and perpendicular to the c -axis. From Fig. 1(f), we notice an increase in ρ_{zx} from 320 K down to 260 K, which then instantaneously become nearly zero below 260 K. This sudden decrease in ρ_{zx} at 260 K coincides with the spin-reorientation transition temperature of the studied sample. The observation of drastic changes in the ρ_{zx} Hall resistivity at 260 K is in good agreement with previous studies on a similar system except for a slightly higher transition temperature of 270 K [32] and 275 K [31]. On the other hand, we observe no significant change in ρ_{xy} from 320 K down to 2 K, which is nearly zero all the time. Next, Fig. 1(g) depicts ρ_{xy} and ρ_{zx} Hall resistivity plotted as a function of temperature for $\text{Mn}_{2.8}\text{Fe}_{0.2}\text{Sn}$ measured with magnetic field of 1 T applied parallel and perpendicular to the c -axis. From Fig. 1(g), we notice an increase in ρ_{zx} from 320 K down to 125 K, which gradually decreases with temperature from 125 K down to 40 K, and then saturates below 40 K. The decrease in ρ_{zx} coincides with the spin-reorientation transition temperature of 125 K as observed from the magnetization measurements on the doped sam-

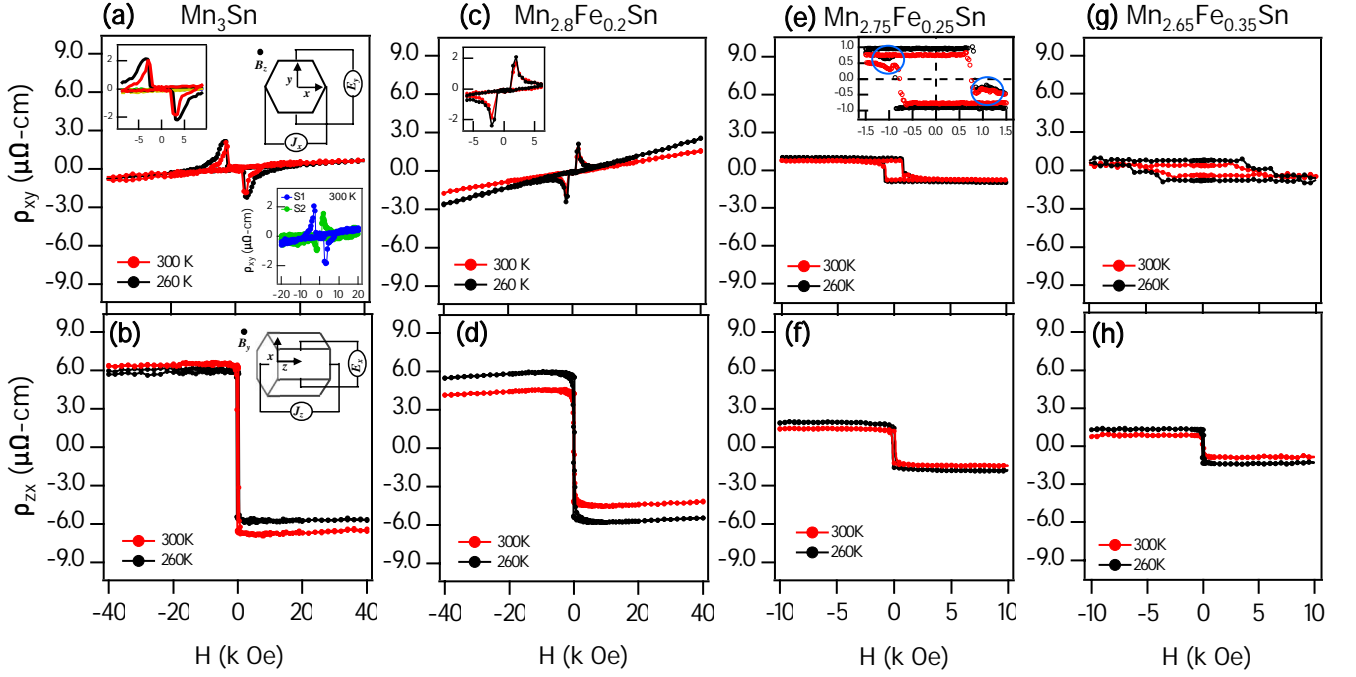


Figure 2. (a) xy -plane (ρ_{xy}) Hall resistivity plotted as a function of the magnetic field from Mn_3Sn . The measuring geometry is shown in the top-right inset of (a) and zoomed-in data at low magnetic fields are shown in the top-left inset of (a). Bottom-right inset in (a) shows the Hall resistance (raw data) measured on two different samples (S1 and S2) of Mn_3Sn at 300 K. (b) zx -plane (ρ_{zx}) Hall resistivity plotted as a function of the magnetic field from Mn_3Sn . The measuring geometry is shown in the top-right inset of (b). (c) and (d), (e) and (f), and (g) and (h) are similar Hall resistivity data of (a) and (b) but measured from $\text{Mn}_{2.8}\text{Fe}_{0.2}\text{Sn}$, $\text{Mn}_{2.75}\text{Fe}_{0.25}\text{Sn}$, and $\text{Mn}_{2.65}\text{Fe}_{0.35}\text{Sn}$, respectively.

ple [see Fig. S1(b) in the supplemental information]. On the other hand, ρ_{xy} slowly increases from 320 K down to 125 K and exponentially increases from 125 K down to 40 K, and then tends to saturate below 40 K. Interestingly, we notice an extremely large ρ_{xy} value of $31 \mu\Omega - \text{cm}$ with 1 T field at 2 K which is negligible in Mn_3Sn .

Fig. 2 shows Hall resistivity, $\rho_{xy}(H)$ for $H \parallel c$ and $\rho_{zx}(H)$ for $H \perp c$, of $\text{Mn}_{3-x}\text{Fe}_x\text{Sn}$ measured at sample temperatures of 260 and 300 K. From Fig. 2(a), we observe that the Hall resistivity (ρ_{xy}) of Mn_3Sn is as high as $2.3 \mu\Omega\text{-cm}$ at 260 K driven by a critical field of 0.3 T which is slightly reduced to $2 \mu\Omega\text{-cm}$ at 300 K. From $\rho_{zx}(H)$ of Mn_3Sn shown in Fig. 2(b), we observe anomalous Hall resistivity (AHR) as high as $6.5 \mu\Omega\text{-cm}$ at 300 K that in good agreement with previous studies on this system [37]. Next, from $\rho_{xy}(H)$ of $\text{Mn}_{2.8}\text{Fe}_{0.2}\text{Sn}$ as shown in Fig. 2(c), we observe Hall resistivity as high as $2 \mu\Omega\text{-cm}$ at 260 K at a critical field of 0.19 T which then reduces to $1.6 \mu\Omega\text{-cm}$ at 300 K. Compared to Mn_3Sn , we notice significant decrease in AHR in $\text{Mn}_{2.8}\text{Fe}_{0.2}\text{Sn}$ [see $\rho_{zx}(H)$ from Fig. 2(d)], particularly at room temperature. Ideally, anomalous Hall effect is not expected in the in-plane Hall resistivity [$\rho_{xy}(H)$] of these systems [16]. But we find non-negligible anomalous Hall signal from the $\rho_{xy}(H)$ data of $\text{Mn}_{2.75}\text{Fe}_{0.25}\text{Sn}$ [see Fig. 2(e)], possibly a component of $\rho_{zx}(H)$ [see Fig. 2(f)] projected due

to difficulties in making perfect Hall connections on the sub-millimeter sized crystals. However, from the zoomed-in $\rho_{xy}(H)$ data of $\text{Mn}_{2.75}\text{Fe}_{0.25}\text{Sn}$ [see inset in Fig. 2(e)] we can clearly identify a cusp in Hall signal (marked by blue circles) at a critical field of 0.1 T. Similarly, Fig. 2(g) shows $\rho_{xy}(H)$ of $\text{Mn}_{2.65}\text{Fe}_{0.35}\text{Sn}$ in which again we find non-negligible anomalous Hall signal coming from $\rho_{zx}(H)$ [see Fig. 2(h)]. Most importantly, we do not find any visible cusp in $\rho_{xy}(H)$ data of $\text{Mn}_{2.65}\text{Fe}_{0.35}\text{Sn}$. Thus, as we go from Mn_3Sn to $\text{Mn}_{2.65}\text{Fe}_{0.35}\text{Sn}$ we can clearly notice two things: i) The intensity of cusp in $\rho_{xy}(H)$ and the critical field at which the cusp appears decrease with increasing Fe doping and ii) Anomalous Hall signal in $\rho_{zx}(H)$ decreases with increasing Fe doping. Particularly, $\rho_{xy}(H)$ and $\rho_{zx}(H)$ of $\text{Mn}_{2.65}\text{Fe}_{0.35}\text{Sn}$ are nearly suppressed at room temperature.

Next, coming to the important results of this study, Figs. 3(a)-(d) show topological Hall resistivity (THR), $\rho_{xy}^T(H)$, of $\text{Mn}_{3-x}\text{Fe}_x\text{Sn}$ ($x=0, 0.2, 0.25$, and 0.35) extracted from the total Hall resistivity [$\rho_{xy}(H)$] shown in Figs. 2(a), 2(c), 2(e), and 2(g), respectively. Note here that the total Hall resistivity shown in Fig. 2 has contributions from normal Hall resistivity (ρ_H^N) which varies linearly with the field ($\rho_H^N = R_0\mu_0 H$), anomalous Hall resistivity (ρ_H^A) which depends on the magnetization ($\rho_H^A = S_A\rho^2 M$), and topological Hall resistivity (ρ_H^T). All

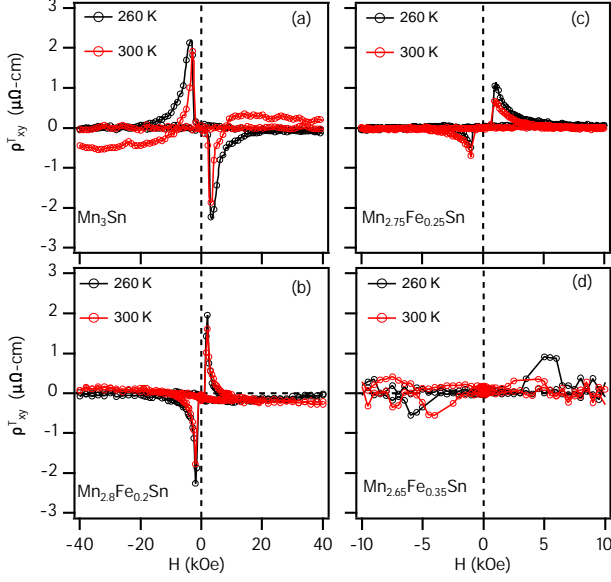


Figure 3. xy -plane topological Hall resistivity (ρ_{xy}^T) plotted as a function of the field from Mn_3Sn (a), $\text{Mn}_{2.8}\text{Fe}_{0.2}\text{Sn}$ (b), $\text{Mn}_{2.75}\text{Fe}_{0.25}\text{Sn}$ (c), and $\text{Mn}_{2.65}\text{Fe}_{0.35}\text{Sn}$ (d).

these contributions lead to a total Hall resistivity as per the relation $\rho_H = \rho_H^N + \rho_H^A + \rho_H^T = R_0\mu_0 H + S_A\rho^2 M + \rho_H^T$. Here R_0 is a normal Hall coefficient and S_A is an anomalous Hall coefficient. To find the topological Hall resistivity one has to subtract the normal and anomalous Hall contributions from the total Hall resistivity, following a method that has been explained thoroughly in several reports [16, 37–39]. However, since the anomalous Hall effect is negligible in ρ_{xy} of these systems, we extracted ρ_{xy}^T by simply subtracting the normal Hall contribution in the case of $x=0$ and $x=0.2$. For $x=0.25$ and $x=0.35$, we extracted ρ_{xy}^T by subtracting the anomalous Hall component originated from $\rho_{zx}(H)$. Overall, Fig. 3 suggests that room temperature ρ_{xy}^T is maximum in Mn_3Sn which then decreases with increase in doping and completely gets suppressed by $x=0.35$ of Fe doping. Moreover, the critical field at which the THE takes places also decreases with increase in doping.

Fig. 4(a) and 4(b) show $\rho_{xy}(H)$ and $\rho_{zx}(H)$ of $\text{Mn}_{2.8}\text{Fe}_{0.2}\text{Sn}$, respectively measured at low temperatures (≤ 150 K). Interestingly, unlike in Mn_3Sn (see Ref. [33] for low temperature data), significant Hall resistivity was found in $\text{Mn}_{2.8}\text{Fe}_{0.2}\text{Sn}$ as high as $36 \mu\Omega\text{-cm}$ at 2 K at an applied field of 4 T. We further observe hysteresis in $\rho_{xy}(H)$ when measured at 2 and 5 K, which is consistent with our magnetization $M(H)$ data [see Fig. S2(c) in the supplemental information]. This suggests that the anomalous Hall resistivity observed in $\text{Mn}_{2.8}\text{Fe}_{0.2}\text{Sn}$ is mostly originated by the Fe-doping induced ferromagnetism [33]. Further, unlike in Mn_3Sn , from Fig. 4(b), we can see finite ρ_{zx} in $\text{Mn}_{2.8}\text{Fe}_{0.2}\text{Sn}$ even at 2 K which increases with temperature. We find

$\rho_{zx} \approx 9.5 \mu\Omega\text{-cm}$ at 150 K. We also notice field-induced asymmetric hysteresis in $\rho_{zx}(H)$ at 2 and 5 K. Observation of asymmetric hysteresis in $\rho_{zx}(H)$ is consistent with the field-induced asymmetric $M(H)$ isotherm measured at 2 K [see Fig. S2(d) in the supplemental information]. Fig. 4(c) depicts $\rho_{xy}^T(H)$ extracted from $\text{Mn}_{2.8}\text{Fe}_{0.2}\text{Sn}$ by following the above discussed technique. While Mn_3Sn shows no topological Hall resistivity in the xy -plane below 260 K, $\text{Mn}_{2.8}\text{Fe}_{0.2}\text{Sn}$ shows topological Hall resistivity as high as $4.5 \mu\Omega\text{-cm}$ at 2 K, which gradually decreases with increasing temperature. But at 100 K, we notice that the sign of ρ_{xy}^T switches from negative to positive for the positive magnetic fields and from positive to negative for the negative magnetic fields as shown in Figs. 4(c). Fig. 4(d) shows the normal Hall coefficient (R_0) and the anomalous Hall coefficient (S_A) plotted as a function of temperature, from which we notice negative normal Hall coefficient at low temperatures, suggesting for dominant electron carriers and at high temperatures R_0 becomes positive due to dominant hole carriers. The normal Hall coefficient sign switching is in-line with the sign change observed in the topological Hall resistivity [see Fig. 4(c)]. Further, the anomalous Hall coefficient gradually decreases with increasing temperature from 0.18 V^{-1} at 2 K to 0.01 V^{-1} at 150 K and beyond 150 K S_A is temperature independent.

Overall, the room-temperature pure and large topological Hall effect observed in Mn_3Sn is an important discovery of this study as to date no other system shows ρ_{xy}^T as high as $2 \mu\Omega\text{-cm}$ at 300 K for such a low critical field of 0.3 T. Moreover, earlier studies on Mn_3Sn reported topological Hall resistivity, ρ_{xy}^T , in the range of $0.3 - 2.1 \mu\Omega\text{-cm}$ besides large anomalous Hall signal [32, 40, 41]. Also, a few systems other than Mn_3Sn show room-temperature THE but again with coexisting AHE. For instance, noncollinear ferromagnet LaMn_2Ge_2 shows topological Hall resistivity of $\approx 1 \mu\Omega\text{-cm}$, in addition to a comparable anomalous Hall resistivity of $0.5 \mu\Omega\text{-cm}$ at 300 K [42]. Frustrated Kagome ferromagnet, Fe_3Sn_2 , shows topological Hall resistivity of $2 \mu\Omega\text{-cm}$ besides a large anomalous Hall resistivity of $4.5 \mu\Omega\text{-cm}$ at 300 K [43]. Similarly, there exists many chiral and skyrmionic systems such as CrTe_2 [44], NiMnGa [45], Mn_2PtSn [46], and YMn_6Sn_6 [47] showing room-temperature topological Hall resistivity with a significant AHE signal. So far, Gd_2PdSi_3 is the only system showing a large topological Hall resistivity of $2.5 \mu\Omega\text{-cm}$, with negligible AHE signal, but at very low-temperatures (< 25 K) [30]. Interestingly, $\text{Mn}_{2.8}\text{Fe}_{0.2}\text{Sn}$ also show pure room-temperature THE with $\rho_{xy}^T \approx 1.6 \mu\Omega\text{-cm}$ at a critical field of 0.2 T, which then increases up to $\approx 4.5 \mu\Omega\text{-cm}$ with decreasing temperature down to 2 K at a critical field of 1.7 T. Note here that the low temperature THE in $\text{Mn}_{2.8}\text{Fe}_{0.2}\text{Sn}$ is coexisted with AHE.

Topological Hall resistivity has been observed in many skyrmionic [9–11, 30] and non-coplanar spin-structured

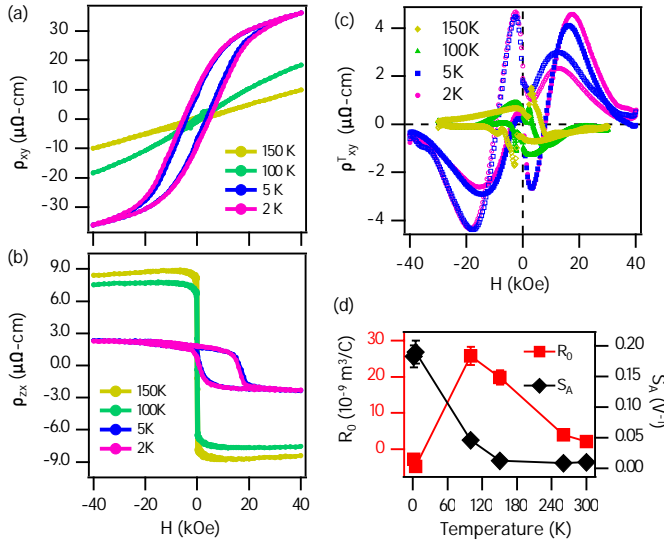


Figure 4. Low temperature (≤ 150 K) Hall resistivity of $\text{Mn}_{2.8}\text{Fe}_{0.2}\text{Sn}$ plotted as a function of field from the xy -plane (a) and zx -plane (b). (c) topological Hall resistivity (ρ_{xy}^T) plotted as a function of the field. (d) Normal Hall coefficient (R_0) and anomalous Hall coefficient (S_A) are plotted as a function of temperature (see the text for more details).

systems [42, 47–49]. There exist various proposals to understand the stabilization of the skyrmion lattice in solids such as (i) DM interaction in noncentrosymmetric systems [17, 50, 51], (ii) uniaxial magnetocrystalline anisotropy in the centrosymmetric systems [52–55], and (iii) in the systems with chiral domain walls [56–59]. Based on our experimental findings, we propose that the clean room-temperature xy -plane THE signal found in $\text{Mn}_{3-x}\text{Fe}_x\text{Sn}$ for $x=0, 0.2, 0.25$ is originated either from the real-space Berry phase due to skyrmion lattice generated from the field-induced domain walls (DW) [32, 40, 41, 56] or from the non-coplanar spin structure [9–11, 30]. However, the low-temperature large THE found in $\text{Mn}_{2.8}\text{Fe}_{0.2}\text{Sn}$ and in other Fe doped systems ($x=0.25$ and 0.35 , reported separately in [33]) could be originated from the magnetocrystalline anisotropy induced by Fe doping [33, 54, 60].

In summary, for the first time, we show a room-temperature pure in-plane topological Hall effect in $\text{Mn}_{3-x}\text{Fe}_x\text{Sn}$ which decreases with increasing Fe doping and is suppressed by a doping concentration of $x=0.35$. We show that the room-temperature topological properties are highly anisotropic in these systems. We also discovered that a small amount of Fe doping in Mn_3Sn causes dramatic changes in the low temperature topological properties. Additional experimental studies using Lorentz transmission electron microscopy (LTEM) would be helpful to map the skyrmionic lattice in these systems. Moreover, our findings demand suitable theoretical models for understanding the high-

temperature topological Hall effect in the Kagome lattice systems.

ACKNOWLEDGEMENTS

Authors thank Science and Engineering Research Board (SERB), Department of Science and Technology (DST), India for the financial support [Grant no. SRG/2020/000393].

* setti@bose.res.in

- [1] E. H. Hall, On a New Action of the Magnet on Electric Currents, in *Semiconductor Devices: Pioneering Papers* (WORLD SCIENTIFIC, 1991) pp. 153–158.
- [2] R. S. Popović, in *Hall Effect Devices* (CRC Press, 2004).
- [3] E. Ramsden, in *Hall-Effect Sensors: Theory and Application* (Elsevier, 2006).
- [4] M. I. Dyakonov and I. V. Perel, Possibility of orientating electron spins with current, *Sov. Phys. JETP Lett.* **13**, 467 (1971).
- [5] R. B. Laughlin, Quantized Hall conductivity in two dimensions, *Phys. Rev. B* **23**, 5632 (1981).
- [6] F. D. M. Haldane, Model for a Quantum Hall Effect without Landau Levels: Condensed-Matter Realization of the "Parity Anomaly", *Phys. Rev. Lett.* **61**, 2015 (1988).
- [7] L. Šmejkal, R. González-Hernández, T. Jungwirth, and J. Sinova, Crystal time-reversal symmetry breaking and spontaneous Hall effect in collinear antiferromagnets, *Sci. Adv.* **6**, eaz8809 (2020).
- [8] R. Karplus and J. M. Luttinger, Hall Effect in Ferromagnetics, *Phys. Rev.* **95**, 1154 (1954).
- [9] P. Bruno, V. K. Dugaev, and M. Taillefumier, Topological Hall Effect and Berry Phase in Magnetic Nanostructures, *Phys. Rev. Lett.* **93**, 096806 (2004).
- [10] M. Lee, W. Kang, Y. Onose, Y. Tokura, and N. P. Ong, Unusual Hall Effect Anomaly in MnSi under Pressure, *Phys. Rev. Lett.* **102**, 186601 (2009).
- [11] A. Neubauer, C. Pfleiderer, B. Binz, A. Rosch, R. Ritz, P. G. Niklowitz, and P. Böni, Topological Hall Effect in the A Phase of MnSi, *Phys. Rev. Lett.* **102**, 186602 (2009).
- [12] T. Moriya, Anisotropic Superexchange Interaction and Weak Ferromagnetism, *Phys. Rev.* **120**, 91 (1960).
- [13] G. Shirane, R. Cowley, C. Majkrzak, J. B. Sokoloff, B. Pagonis, C. H. Perry, and Y. Ishikawa, Spiral magnetic correlation in cubic mnsi, *Phys. Rev. B* **28**, 6251 (1983).
- [14] S. Tomiyoshi and Y. Yamaguchi, Magnetic Structure and Weak Ferromagnetism of Mn3Sn Studied by Polarized Neutron Diffraction, *J. Phys. Soc. Japan* **51**, 2478 (1982).
- [15] J. Sticht, K.-H. Höck, and J. Kübler, Non-collinear itinerant magnetism: the case of Mn_3Sn , *Journal of Physics: Condensed Matter* **1**, 8155 (1989).
- [16] S. Nakatsuji, N. Kiyohara, and T. Higo, Large anomalous Hall effect in a non-collinear antiferromagnet at room temperature, *Nature* **527**, 212 (2015).
- [17] P. Park, J. Oh, K. Uhlířová, J. Jackson, A. Deák, L. Szunyogh, K. H. Lee, H. Cho, H.-L. Kim, H. C. Walker,

- et al.*, Magnetic excitations in non-collinear antiferromagnetic Weyl semimetal Mn_3Sn , npj Quantum Materials **3**, 63 (2018).
- [18] N. Morali, R. Batabyal, P. K. Nag, E. Liu, Q. Xu, Y. Sun, B. Yan, C. Felser, N. Avraham, and H. Beidenkopf, Fermi-Arc diversity on surface terminations of the magnetic Weyl semimetal $\text{Co}_3\text{Sn}_2\text{S}_2$, Science **365**, 1286 (2019).
- [19] Y. Okamura, S. Minami, Y. Kato, Y. Fujishiro, Y. Kaneko, J. Ikeda, J. Muramoto, R. Kaneko, K. Ueda, V. Kocsis, N. Kanazawa, Y. Taguchi, T. Koretsune, K. Fujiwara, A. Tsukazaki, R. Arita, Y. Tokura, and Y. Takahashi, Giant magneto-optical responses in magnetic Weyl semimetal $\text{Co}_3\text{Sn}_2\text{S}_2$, Nat. Commun. **11**, 4619 (2020).
- [20] S. Baidya, A. V. Mallik, S. Bhattacharjee, and T. Saha-Dasgupta, Interplay of Magnetism and Topological Superconductivity in Bilayer Kagome Metals, Phys. Rev. Lett. **125**, 026401 (2020).
- [21] L. D. Sanjeewa, J. Xing, K. M. Taddei, D. Parker, R. Custelcean, C. dela Cruz, and A. S. Sefat, Evidence of Ba-substitution induced spin-canting in the magnetic Weyl semimetal EuCd_2As_2 , Phys. Rev. B **102**, 104404 (2020).
- [22] Muhlbauer, S. and Binz, B. and Jonietz, F. and Pfleiderer, C. and Rosch, A. and Neubauer, A. and Georgii, R. and Boni, P., Skyrmion Lattice in a Chiral Magnet, Science **323**, 915 (2009).
- [23] X. Z. Yu, N. Kanazawa, Y. Onose, K. Kimoto, W. Z. Zhang, S. Ishiwata, Y. Matsui, and Y. Tokura, Near room-temperature formation of a skyrmion crystal in thin-films of the helimagnet FeGe , Nature Materials **10**, 106 (2010).
- [24] T. Tanigaki, K. Shibata, N. Kanazawa, X. Yu, Y. Onose, H. S. Park, D. Shindo, and Y. Tokura, Real-Space Observation of Short-Period Cubic Lattice of Skyrmions in MnGe , Nano Letters **15**, 5438 (2015).
- [25] O. Janson, I. Rousochatzakis, A. A. Tsirlin, M. Belesi, A. A. Leonov, U. K. Rößler, J. van den Brink, and H. Rosner, The quantum nature of skyrmions and half-skyrmions in Cu_2OSeO_3 , Nature Communications **5**, 10.1038/ncomms6376 (2014).
- [26] K. G. Rana and O. Meshcheriakova and J. Kübler and B. Ernst and J. Karel and R. Hillebrand and E. Pippel and P. Werner and A. K. Nayak and C. Felser and S. S. P. Parkin, Observation of topological Hall effect in Mn_2RhSn films, New Journal of Physics **18**, 085007 (2016).
- [27] Q. Shao, Y. Liu, G. Yu, S. K. Kim, X. Che, C. Tang, Q. L. He, Y. Tserkovnyak, J. Shi, and K. L. Wang, Topological Hall effect at above room temperature in heterostructures composed of a magnetic insulator and a heavy metal, Nature Electronics **2**, 182 (2019).
- [28] S. Luo and L. You, Skyrmion devices for memory and logic applications, APL Materials **9**, 050901 (2021).
- [29] M. J. Gilbert, Topological electronics, Communications Physics **4**, 10.1038/s42005-021-00569-5 (2021).
- [30] T. Kurumaji, T. Nakajima, M. Hirschberger, A. Kikkawa, Y. Yamasaki, H. Sagayama, H. Nakao, Y. Taguchi, T.-h. Arima, and Y. Tokura, Skyrmion lattice with a giant topological Hall effect in a frustrated triangular-lattice magnet, Science **365**, 914 (2019).
- [31] N. H. Sung, F. Ronning, J. D. Thompson, and E. D. Bauer, Magnetic phase dependence of the anomalous Hall effect in Mn_3Sn single crystals, Appl. Phys. Lett. **112**, 132406 (2018).
- [32] J. Yan, X. Luo, H. Y. Lv, Y. Sun, P. Tong, W. J. Lu, X. B. Zhu, W. H. Song, and Y. P. Sun, Room-temperature angular-dependent topological Hall effect in chiral antiferromagnetic Weyl semimetal Mn_3Sn , Appl. Phys. Lett. **115**, 102404 (2019).
- [33] A. Low, S. Ghosh, S. Changdar, S. Routh, S. Purwar, and S. Thirupathaiah, Tuning of topological properties in the strongly correlated antiferromagnet Mn_3Sn via Fe doping, Phys. Rev. B **106**, 144429 (2022).
- [34] L. Xu, X. Li, X. Lu, C. Collignon, H. Fu, J. Koo, B. Fauqué, B. Yan, Z. Zhu, and K. Behnia, Finite-temperature violation of the anomalous transverse Wiedemann-Franz law, Sci. Adv. **6**, eaaz3522 (2020).
- [35] C. Barone, F. Romeo, A. Galdi, P. Orgiani, L. Maritato, A. Guarino, A. Nigro, and S. Pagano, Universal origin of unconventional $1/f$ noise in the weak-localization regime, Phys. Rev. B **87**, 245113 (2013).
- [36] S. Tomiyoshi, H. Yoshida, H. Ohmori, T. Kaneko, and H. Yamamoto, Electrical properties of the intermetallic compound Mn_3Sn , J. Magn. Magn. Mater. **70**, 247 (1987).
- [37] P. K. Rout, P. V. P. Madduri, S. K. Manna, and A. K. Nayak, Field-induced topological Hall effect in the noncoplanar triangular antiferromagnetic geometry of Mn_3Sn , Phys. Rev. B **99**, 094430 (2019).
- [38] N. Kanazawa, Y. Onose, T. Arima, D. Okuyama, K. Ohoyama, S. Wakimoto, K. Kakurai, S. Ishiwata, and Y. Tokura, Large Topological Hall Effect in a Short-Period Helimagnet MnGe , Phys. Rev. Lett. **106**, 156603 (2011).
- [39] K. Kuroda, T. Tomita, M.-T. Suzuki, C. Bareille, A. Nugroho, P. Goswami, M. Ochi, M. Ikhlas, M. Nakayama, S. Akebi, R. Noguchi, R. Ishii, N. Inami, K. Ono, H. Kumigashira, A. Varykhalov, T. Muro, T. Koretsune, R. Arita, S. Shin, T. Kondo, and S. Nakatsuji, Evidence for magnetic Weyl fermions in a correlated metal, Nat. Mater. **16**, 1090 (2017).
- [40] X. Li, L. Xu, H. Zuo, A. Subedi, Z. Zhu, and K. Behnia, Momentum-space and real-space Berry curvatures in Mn_3Sn , SciPost Physics **5**, 063 (2018).
- [41] X. Li, C. Collignon, L. Xu, H. Zuo, A. Cavanna, U. Gennser, D. Mailly, B. Fauqué, L. Balents, Z. Zhu, and K. Behnia, Chiral domain walls of Mn_3Sn and their memory, Nat. Commun. **10**, 3021 (2019).
- [42] G. Gong, L. Xu, Y. Bai, Y. Wang, S. Yuan, Y. Liu, and Z. Tian, Large topological Hall effect near room temperature in noncollinear ferromagnet LaMn_2Ge_2 single crystal, Phys. Rev. Materials **5**, 034405 (2021).
- [43] Q. Wang, Q. Yin, and H. Lei, Giant topological Hall effect of ferromagnetic kagome metal Fe_3Sn_2 , Chin. Phys. B **29**, 017101 (2020).
- [44] M. Huang, L. Gao, Y. Zhang, X. Lei, G. Hu, J. Xiang, H. Zeng, X. Fu, Z. Zhang, G. Chai, Y. Peng, Y. Lu, H. Du, G. Chen, J. Zang, and B. Xiang, Possible Topological Hall Effect above Room Temperature in Layered $\text{Cr}_1.2\text{Te}_2$ Ferromagnet, Nano Letters **21**, 4280 (2021).
- [45] W. Zhang, B. Balasubramanian, A. Ullah, R. Pahari, X. Li, L. Yue, S. R. Valloppilly, A. Sokolov, R. Skomski, and D. J. Sellmyer, Comparative study of topological Hall effect and skyrmions in NiMnIn and NiMnGa , Applied Physics Letters **115**, 172404 (2019).
- [46] Y. Li, B. Ding, X. Wang, H. Zhang, W. Wang, and Z. Liu, Large topological hall effect observed in tetrago-

- nal Mn₂PtSn Heusler thin film, *Appl. Phys. Lett.* **113**, 062406 (2018).
- [47] N. J. Ghimire, R. L. Dally, L. Poudel, D. C. Jones, D. Michel, N. T. Magar, M. Bleuel, M. A. McGuire, J. S. Jiang, J. F. Mitchell, J. W. Lynn, and I. I. Mazin, Competing magnetic phases and fluctuation-driven scalar spin chirality in the kagome metal YMn₆Sn₆, *Sci. Adv.* **6**, eabe2680 (2020).
- [48] Y. Shiomi, S. Iguchi, and Y. Tokura, Emergence of topological Hall effect from fanlike spin structure as modified by Dzyaloshinsky-Moriya interaction in MnP, *Phys. Rev. B* **86**, 180404 (2012).
- [49] S. Roychowdhury, S. Singh, S. N. Guin, N. Kumar, T. Chakraborty, W. Schnelle, H. Borrmann, C. Shekhar, and C. Felser, Giant Topological Hall Effect in the Noncollinear Phase of Two-Dimensional Antiferromagnetic Topological Insulator MnBi₄Te₇, *Chemistry of Materials* **33**, 8343 (2021), <https://doi.org/10.1021/acs.chemmater.1c02625>.
- [50] N. Kanazawa, M. Kubota, A. Tsukazaki, Y. Kozuka, K. S. Takahashi, M. Kawasaki, M. Ichikawa, F. Kagawa, and Y. Tokura, Discretized topological Hall effect emerging from skyrmions in constricted geometry, *Phys. Rev. B* **91**, 041122 (2015).
- [51] J. Liu and L. Balents, Anomalous Hall Effect and Topological Defects in Antiferromagnetic Weyl Semimetals: Mn₃Sn/Ge, *Phys. Rev. Lett.* **119**, 087202 (2017).
- [52] X. Yu, Y. Tokunaga, Y. Kaneko, W. Zhang, K. Kimoto, Y. Matsui, Y. Taguchi, and Y. Tokura, Biskyrmion states and their current-driven motion in a layered manganite, *Nature Communications* **5**, 1 (2014).
- [53] Z. Hou, W. Ren, B. Ding, G. Xu, Y. Wang, B. Yang, Q. Zhang, Y. Zhang, E. Liu, F. Xu, W. Wang, G. Wu, X. Zhang, B. Shen, and Z. Zhang, Observation of Various and Spontaneous Magnetic Skyrmionic Bubbles at Room Temperature in a Frustrated Kagome Magnet with Uniaxial Magnetic Anisotropy, *Adv. Mater.* **30**, 1706306 (2018).
- [54] X. Yu, M. Mostovoy, Y. Tokunaga, W. Zhang, K. Kimoto, Y. Matsui, Y. Kaneko, N. Nagaosa, and Y. Tokura, Magnetic stripes and skyrmions with helicity reversals, *Proc. Natl. Acad. Sci.* **109**, 8856 (2012).
- [55] M. Preißinger, K. Karube, D. Ehlers, B. Szigeti, H.-A. Krug von Nidda, J. S. White, V. Ukleev, H. M. Rønnow, Y. Tokunaga, A. Kikkawa, Y. Tokura, Y. Taguchi, and I. Kézsmárki, Vital role of magnetocrystalline anisotropy in cubic chiral skyrmion hosts, *npj Quantum Materials* **6**, 10.1038/s41535-021-00365-y (2021).
- [56] S. B. Gudnason and M. Nitta, Domain Wall Skyrmions, *Phys. Rev. D* **89**, 085022 (2014).
- [57] R. Cheng, M. Li, A. Sapkota, A. Rai, A. Pokhrel, T. Mewes, C. Mewes, D. Xiao, M. De Graef, and V. Sokalski, Magnetic domain wall skyrmions, *Phys. Rev. B* **99**, 184412 (2019).
- [58] T. Nagase, Y.-G. So, H. Yasui, T. Ishida, H. K. Yoshida, Y. Tanaka, K. Saitoh, N. Ikarashi, Y. Kawaguchi, M. Kuwahara, and M. Nagao, Observation of domain wall bimerons in chiral magnets, *Nat. Commun.* **12**, 10.1038/s41467-021-23845-y (2021).
- [59] K. Yang, K. Nagase, Y. Hirayama, T. D. Mishima, M. B. Santos, and H. Liu, Wigner solids of domain wall skyrmions, *Nat. Commun.* **12**, 10.1038/s41467-021-26306-8 (2021).
- [60] S. Hayami, S.-Z. Lin, and C. D. Batista, Bubble and skyrmion crystals in frustrated magnets with easy-axis anisotropy, *Phys. Rev. B* **93**, 184413 (2016).